Breaking wave interaction with tandem cylinders under different impact scenarios

Hans Bihs*, Arun Kamath, Mayilvahanan Alagan Chella, Øivind A. Arntsen

Department of Civil and Environmental Engineering, Norwegian University of Science and Technology (NTNU), 7491 Trondheim, Norway

Journal of Waterway, Port, Coastal, and Ocean Engineering, 2016, **142** (5), pp. 04016005-1–14.
DOI: http://dx.doi.org/10.1061/(ASCE)WW.1943-5460.0000343

Abstract

The interaction of plunging breaking waves with a pair of cylinders placed in tandem is investigated using the open-source computational fluid dynamics (CFD) model REEF3D. The model is validated using experimental data for total wave forces and free surface elevations for breaking wave interaction with a single cylinder. Wave interaction with tandem cylinders is investigated for four different wave impact scenarios on the first cylinder and six different distances between the cylinders in each scenario. Wave forces on the upstream cylinder are generally found to be less than the forces on a single cylinder for a particular scenario. The force on the downstream cylinder is lower than the force on the upstream cylinder when the breaker tongue impacts the first cylinder. Under conditions where the breaker tongue impacts the downstream cylinder around the wave crest level, the wave force on the downstream cylinder is higher than the force on the upstream cylinder. The wave forces experienced by the tandem cylinders is highly influenced by the location of the breaking point with respect to the cylinders and the distance between the cylinders.

Keywords: Breaking-waveforces; Verticalcylinder; Tandemcylinders; Computational Fluid Dynamics; REEF3D

1 Introduction

The interaction of breaking wave forces on structures involves complex two-phase air-water interaction, rapid free surface deformations and an impulsive force. The short duration over which these interactions occur, pose several challenges to the evaluation of breaking wave

*Corresponding author, hans.bihs@ntnu.no

Postprint, published in Journal of Waterway, Port, Coastal, and Ocean Engineering, doi: http://dx.doi.org/10.1061/(ASCE)WW.1943-5460.0000343

forces. In shallow waters, the hydrodynamic loading on structures such as offshore wind turbine substructures is mostly governed by the loading due to plunging breaking waves (Alagan Chella et al., 2012). The theoretical description of breaking waves in shallow waters is rather limited up to the transition region close to breaking. The evolution of the breaking process and the underlying flow physics can not be described theoretically. This is due to the simplifying assumptions of single-phase and two-dimensional flow, irrotational motion, no return flow and hydrostatic pressure made in obtaining analytical solutions (Cokelet, 1977).

The current knowledge on breaking wave kinematics is mainly based on experimental investigations. Deep water breaking waves were studied by Kjeldsen and Myrhaug (1978); Battjes and Sakai (1981); Bonmarin (1989); Rapp and Melville (1990) and Duncan (2001). Wave breaking on plane beaches was studied by Stive and Wind (1982); Miller (1987); Nadaoka et al. (1989) and Ting and Kim (1994) while wave breaking over submerged structures was studied by Gourlay (1994); Smith and Kraus (1990) and Blenkinsopp and Chaplin (2008). While these studies focussed on the kinematics and dynamics of breaking waves, several other researchers experimentally investigated breaking wave forces on cylinders, e.g. Goda et al. (1966); Watanabe and Horikawa (1974); Apelt and Piorewicz (1986); Chan and Melville (1988); Sawaragi and Nochino (1984); Chaplin et al. (1992); Wienke et al. (2000) and Arntsen et al. (2011). However, the measurement of the quantities related to the wave breaking and their interaction with structures is challenging.

Theoretically, the total breaking wave force on a vertical slender cylinder can be expressed in terms of a slowly varying quasi-static force and an impulsive wave impact force. Goda et al. (1966) proposed the use of an impact force term in addition to the quasi-static force predicted by the Morison formula (Morison et al., 1950) to evaluate breaking wave forces. The impact force characteristics are mainly determined by the geometric properties and kinematics at breaking, such as the shape of the wave and the distribution of water particle velocities under the wave crest (Goda et al., 1966).

Watanabe and Horikawa (1974) investigated breaking wave forces on a large cylinder and proposed a formula that includes the phase difference between the water particle acceleration and the inertia force. They also pointed out that empirical coefficients used to calculate breaking wave forces are not universal and depend on breaking wave characteristics. Apelt and Piorewicz (1986) carried out experiments to study interference effects of breaking wave forces on rows of two or three vertical cylinders placed along and normal to the direction of wave propagation. Their results suggested that both the distance between the cylinders and the incident wave steepness are important factors when in a row is arranged normal to the direction of wave propagation. They further concluded that the separation distance does not significantly influence the wave forces when the row is along the direction of wave propagation. Sparboom et al. (2005) studied breaking wave forces due to freak waves on two and three cylinder arrays and found that breaking wave forces are reduced significantly along the array due to a sheltering effect from upstream cylinders.

Wienke et al. (2000) carried out large-scale studies on breaking wave impact on a single slender cylinder and presented different wave loading cases that considered the position of the cylinder with respect to the wave breaking point. Irschik et al. (2002) extended this work and presented the Empirical Mode Decomposition (EMD) method to separate the slowly varying quasi-static loading and the dynamic response of the cylinder from the measured breaking wave force history. Based on their large-scale investigations, Wienke and Oumeraci (2005) proposed a theoretical model to calculate breaking wave forces on a single slender cylinder

using the wave celerity and curling factor as inputs.

The curling factor (λ) is a parameter used to determine the contribution of the wave crest to the wave impact force during breaking. The values for λ are determined experimentally for different bottom slopes and water depths, and these values depend on the breaker type. According to Wienke and Oumeraci (2005), the wave impact scenario is different for different distances between the cylinder surface and the breaking point. While calculating λ, the assumption of instantaneous wave impact on the cylinder can also lead to overestimating the breaking wave force. Hildebrandt and Schlurmann (2012) investigated breaking wave forces on a tripod structure in large-scale experiments to study the detailed temporal and spatial variations in the wave slamming loads. They concluded that the curling factors, vertical position of impact and maximum slamming coefficients increase as the distance between the cylinder and the point of wave breaking decreases. Their results agreed with the theoretical slamming coefficients given by Goda et al. (1966).

Most of the current approaches to evaluate breaking wave forces strongly depend on experimentally determined coefficients. However, the measuring various parameters such as velocity and acceleration during breaking is a challenging task (Arntsen et al., 2011). Also, the coefficients are valid only for cases that are similar to the experiments used to obtain them and cannot be applied with multiple cylinders and different arrangements of the cylinders. In addition, the distance from the cylinder to the breaking point results in several breaking wave interaction scenarios that have to be studied in detail to gain useful insights into the breaking wave-structure interaction problem.

Computational fluid dynamics (CFD) models can evaluate breaking waves with few assumptions about the fluid physics to obtain detailed insights into the breaking wave-structure interaction (Christensen, 1998). Many numerical studies have been carried out to investigate the breaking process in shallow waters with single-phase CFD models (Lin and Liu, 1998; Bradford, 2000; Christensen and Deigaard, 2001; Zhao et al., 2004). Hieu et al. (2004) showed that a two-phase CFD model better resolves the breaking wave kinematics. Thus, two-phase CFD models in recent literature include the air-water interaction in the modeling (Chen et al., 1999; Christensen, 2006; Wang et al., 2009; Jacobsen et al., 2012; Xie, 2013; Alagan Chella et al., 2015*b*). In addition, results from Alagan Chella et al. (2015*b*) and Alagan Chella et al. (2015*a*) show that higher order discretization schemes, tight velocity-pressure coupling and a sharp representation of the free surface provide a more realistic description of the breaking waves. These studies have advanced the knowledge in current literature regarding breaking wave kinematics.

Bredmose and Jacobsen (2010) carried out simulations of focussed wave breaking forces on a slender cylinder using the open-source CFD model OpenFOAM without an explicit turbulence model, using half of the computational domain and assuming lateral symmetry in the flow field. Mo et al. (2013) investigated solitary wave breaking over a slope and its interaction with a slender cylinder with experiments and a CFD model assuming lateral symmetry. For the free surface elevations and particle velocities, the experimental and numerical results showed good agreement. Choi et al. (2015) studied the free surface elevation and breaking wave forces on vertical and inclined single cylinders using a CFD model. Good agreement was obtained between the computed results and the filtered experimental data. However, numerical investigations of breaking wave forces on tandem cylinders, the effect of neighboring cylinders on breaking wave forces, and the complex free surface deformations associated with this interaction has not been presented in current literature to our knowledge.

The interaction between breaking waves and a cylinder involves several important free surface features such as runup on the cylinder, separation of the breaking wavefront around the cylinder, formation of a water jet behind the cylinder and the rejoining of the separated wavefront behind the cylinder. In the presence of neighboring cylinders, the scenario is further relevant as it represents coastal and offshore constructions. In this study, the open-source CFD model REEF3D is used to evaluate breaking wave forces on tandem cylinders placed at different distances from each other in a three-dimensional numerical wave tank. The model has been previously used to investigate breaking wave kinematics (Alagan Chella et al., 2015*b*) and to calculate non-breaking wave forces on tandem cylinders (Kamath et al., 2015). Several free surface features and wave impact scenarios associated with breaking waves interacting with a single cylinder and the resulting forces on the cylinder have been discussed in current literature. This paper investigates the case of two cylinders placed in tandem, focussing on how the distance between the cylinders influences the wave forces and the flow features around the cylinders. Four different wave impact scenarios and six separation distances between cylinders are considered. The numerical model is validated using experimental results from the Large Wave Flume (GWK) (Irschik et al., 2002) for breaking wave interaction with a single cylinder.

2 Numerical Model

2.1 Governing equations

The numerical wave tank REEF3D solves the incompressible three-dimensional Reynolds-Averaged Navier-Stokes (RANS) equations:

$$\frac{\partial u_i}{\partial x_i} = 0 \tag{1}$$

$$\frac{\partial u_i}{\partial t} + u_j \frac{\partial u_i}{\partial x_j} = -\frac{1}{\rho}\frac{\partial p}{\partial x_i} + \frac{\partial}{\partial x_j}\left[(\nu + \nu_t)\left(\frac{\partial u_i}{\partial x_j} + \frac{\partial u_j}{\partial x_i}\right)\right] + g_i \tag{2}$$

where u is the velocity, ρ is the density of the fluid, p is the pressure, ν is the kinematic viscosity, ν_t is the eddy viscosity and g the acceleration due to gravity.

The fifth-order conservative finite difference Weighted Essentially Non-Oscillatory (WENO) scheme proposed by Jiang and Shu (1996) is applied to discretize the convective terms of the RANS equation. Time is advanced using a Total Variation Diminishing (TVD) third-order Runge-Kutta explicit time scheme (Shu and Osher, 1988). The time step size is controlled with adaptive time stepping based on the Courant-Friedrichs-Lewy (CFL) criterion; this results in an optimal time step value for numerical stability and accuracy. Diffusion is treated with an implicit time scheme to exclude it from the CFL criterion. Pressure is treated with the projection method (Chorin, 1968). The Poisson equation for pressure is solved with the preconditioned BiCGStab solver (van der Vorst, 1992). The domain decomposition strategy and MPI (Message Passing Interface) is used for parallelization. A Cartesian grid with a staggered arrangement is used in the numerical model. Complex geometries are taken into account with the ghost cell immersed boundary method (Berthelsen and Faltinsen, 2008).

The k-ω model is employed for turbulence closure (Wilcox, 1994) with transport equations for the turbulent kinetic energy k and the specific turbulence dissipation ω shown in Eqs. (3)

and (4) respectively. Wall functions are used for k and ω.

$$\frac{\partial k}{\partial t} + u_j \frac{\partial k}{\partial x_j} = \frac{\partial}{\partial x_j}\left[\left(\nu + \frac{\nu_t}{\sigma_k}\right)\frac{\partial k}{\partial x_j}\right] + P_k - \beta_k k\omega \tag{3}$$

$$\frac{\partial \omega}{\partial t} + u_j \frac{\partial \omega}{\partial x_j} = \frac{\partial}{\partial x_j}\left[\left(\nu + \frac{\nu_t}{\sigma_\omega}\right)\frac{\partial \omega}{\partial x_j}\right] + \frac{\omega}{k}\alpha P_k - \beta\omega^2 \tag{4}$$

where, eddy viscosity $\nu_t = k/\omega$, P_k is the production rate, and the closure coefficients $\sigma_k = 2$, $\sigma_\omega = 2$, $\alpha = 5/9$, $\beta_k = 9/100$, $\beta = 3/40$. Eddy viscosity limiters (Durbin, 2009) are used to control the overproduction of turbulence, often occurring in highly unsteady free surface flows. In addition, because the turbulence length scales cannot pass the water-air interface, a free surface turbulence damping scheme is considered (Naot and Rodi, 1982).

2.2 Free Surface

The complex wave hydrodynamics are modeled with a two-phase flow approach, calculating the flows for water and air. The interface between the two fluids is captured with the level set method (Osher and Sethian, 1988). The zero level set of the signed distance function $\phi(\vec{x}, t)$ represents the location of the free surface. With its signed distance property, it gives the shortest distance from the interface to all the points in the flow domain. Based on the sign of the level set function, the phases can be distinguished as follows:

$$\phi(\vec{x}, t)\begin{cases} > 0 & if\ \vec{x}\ is\ in\ phase\ 1 \\ = 0 & if\ \vec{x}\ is\ at\ the\ interface \\ < 0 & if\ \vec{x}\ is\ in\ phase\ 2 \end{cases} \tag{5}$$

The flow velocities calculated from Eq. (2) are used to convect the level set function:

$$\frac{\partial \phi}{\partial t} + u_j \frac{\partial \phi}{\partial x_j} = 0 \tag{6}$$

During computation, reinitialization is carried out after every iteration using a partial differential equation by Peng et al. (1999) in order to maintain the signed distance property of the level set function. The level set function is discretized with the Hamilton-Jacobi formulation of the WENO scheme by Jiang and Peng (2000).

2.3 Wave generation and absorption

The numerical wave tank uses the relaxation method (Larsen and Dancy, 1983) for the wave generation. To moderate the velocity and the free surface, a relaxation function is used in the relaxation zones:

$$\begin{aligned} u_{relaxed} &= \Gamma(x) u_{analytical} + (1 - \Gamma(x)) u_{computational} \\ \phi_{relaxed} &= \Gamma(x) \phi_{analytical} + (1 - \Gamma(x)) \phi_{computational} \end{aligned} \tag{7}$$

where $\Gamma(x)$ is the relaxation function and $x \in [0, 1]$ is the x-coordinate scaled to the length of the relaxation zone. The relaxation function shown in Eq. (8) is used in the current numerical model (Jacobsen et al., 2012):

$$\Gamma(x) = 1 - \frac{e^{(1-x)^{3.5}} - 1}{e - 1} \tag{8}$$

To avoid reflections from the downstream boundary, an active wave absorption method is employed. Here, waves opposite to the reflected ones are generated, canceling out the reflections. Based on shallow water theory (Schäffer and Klopman, 2000), the following horizontal velocity is prescribed on the downstream boundary:

$$u\left(t\right) = -\sqrt{\frac{g}{h}}\,\xi\left(t\right) \tag{9}$$

where

$$\xi\left(t\right) = \eta\left(t\right) - h \tag{10}$$

Here, $\eta\left(t\right)$ is the actual free surface location along the downstream boundary and h the still water level. The method is applied in vertical strips as wide as one grid cell along the downstream boundary. This way, different free surface elevations along the boundary can be taken into account (Higuera et al., 2013). Also, the handling of oblique waves is also implemented in the current model.

2.4 Numerical evaluation of wave forces

The breaking wave forces on the cylinders is calculated by integrating the pressure p and the surface normal component of the viscous shear stress tensor τ on the surface of the solid objects:

$$F = \int_{\Omega} (-\mathbf{n}p + \mathbf{n} \cdot \tau) d\Omega \tag{11}$$

where $\mathbf{n}$ is the unit normal vector pointing into the fluid and Ω is the surface of the object.

3 Results and Discussion

3.1 Validation of the numerical model

The breaking wave force on a single vertical cylinder is calculated numerically and compared to experimental data to validate the numerical model. The experiments were carried out at the Large Wave Flume (GWK) in Hannover, Germany (Irschik et al., 2002) on a vertical cylinder of diameter $D = 0.7$ m in a water depth of 3.80 m with incident waves of period $T = 4.0$ s. The cylinder is placed at the top of a 23 m long 1 : 10 slope, such that the still water depth at the cylinder is 1.50 m. In the numerical setup, the wave tank is 59 m long, 5 m wide and 7 m high with a grid size of $dx = 0.05$ m, resulting in a total of 16.52 million cells. A cylinder with $D = 0.7$ m is placed with its center at 44.0 m, and incident waves of period $T = 4.0$ s break exactly on the front surface of the cylinder. The complete numerical setup is illustrated in Fig. (1a). The definition sketch for tandem cylinders in the wave tank shows the location of the wave gages and the separation distance in Fig. (1b).

The numerically calculated wave force is compared to the EMD (Empirical Mode Decomposition) treated experimental data from Choi et al. (2015) to filter out the dynamic amplification of the wave forces due to vibration of the cylinder as shown in Fig. (2a). Good agreement is seen between the numerical and experimental wave forces. The numerical results are also similar over several wave periods, showing that the numerical model predicts the the

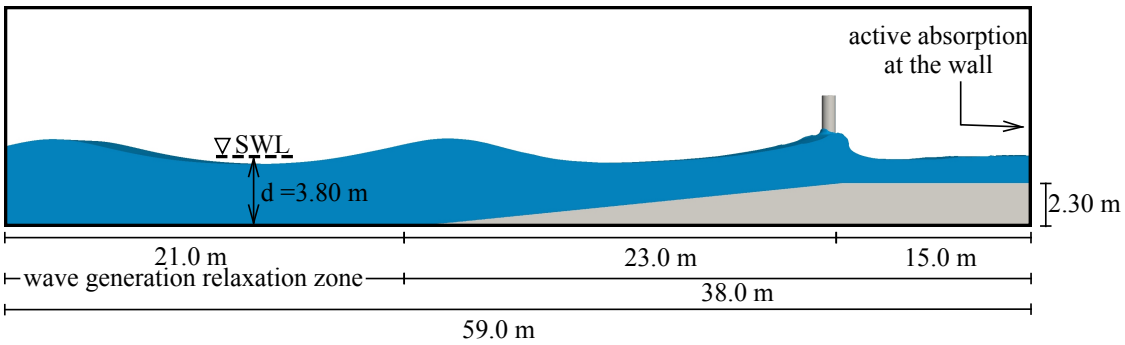

(a) numerical wave tank showing the dimensions of the tank and wave generation and absorption zones

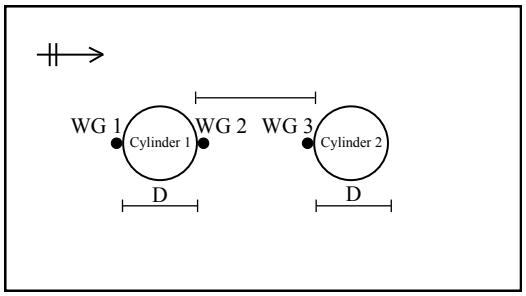

(b) schematic diagram showing the wave gage locations around the cylinders

Figure 1: Numerical wave tank setup used in the study

wave breaking location and consequently the breaking wave forces consistently. The free surface elevation near the wall along the frontline of the cylinder provides a representation of the incident wave on the cylinder. Comparison of the numerical and experimental free surface elevations shows good agreement in Fig. (2b). The vertical wavefront in the figure shows that the wave breaks on the front surface of the cylinder.

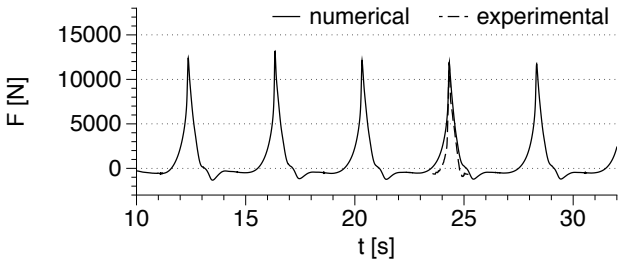

(a) wave force on the cylinder

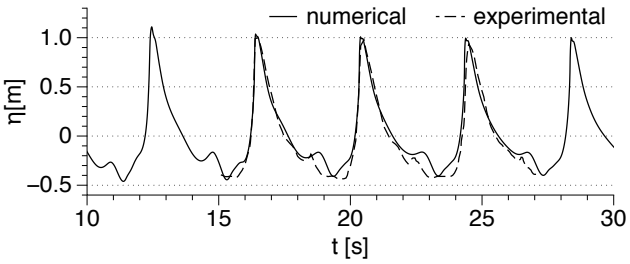

(b) free surface near the wall along the frontline of the cylinder

Figure 2: Comparison of the numerical and experimental results

3.2 Effect of wave impact scenario and distance between tandem cylinders on the wave forces

The wave forces on tandem cylinders placed at different distances from each other are studied for different wave breaking scenarios. The different scenarios are determined by the location of the wave breaking point with respect to the front surface of the first cylinder. The scenarios considered in this study are:

- scenario A: overturning wave crest impacts cylinder 1 just below the wave crest level
- scenario B: overturning wave crest impacts cylinder 1 at the wave crest level
- scenario C: wave breaks exactly at cylinder 1 with a vertical wavefront
- scenario D: wave breaks just behind cylinder 1

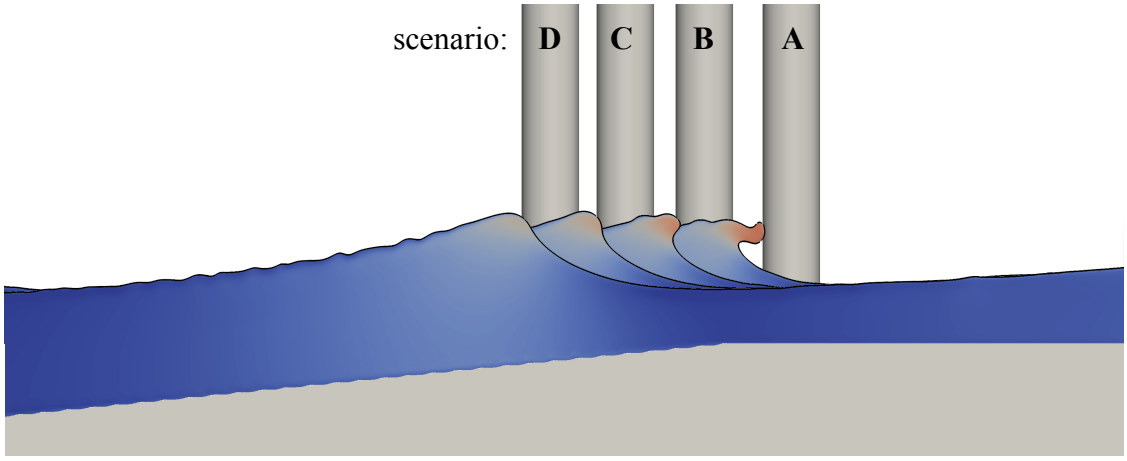

Figure 3: Four different locations of cylinder 1 with respect to the wave breaking point considered in the study

The various scenarios are illustrated in Fig. (3). Simulations are carried out to determine the breaking wave force for a single cylinder F_0 in each scenario. Previous studies dealing with breaking waves on a single slender cylinder have presented that the mode of wave impact on the cylinder due to the distance between the breaking point and the cylinder significantly impacts the wave forces acting on the cylinder. According to Irschik et al. (2002), scenarios A and B result in the highest and the second highest total wave forces on a single cylinder respectively. The lowest wave forces on a single cylinder are obtained in scenario D. In the context of tandem cylinders, the wave impact on cylinder 1 and the separation distance between the two cylinders can influence in the wave forces experienced by both cylinders. This is investigated in this study by placing the second cylinder at separation distances of $S = 1D$, $S = 2D$, $S = 3D$, $S = 4D$, $S = 5D$ and $S = 6D$. The resulting 24 different cases are listed in Table (1) along with the numerical forces calculated for a single cylinder in each of the wave breaking scenarios, F_0. Table (1) also lists the maximum force on each cylinder with respect to F_0 for each case (F_1/F_0 and F_2/F_0) and the maximum wave crest elevations in front of the cylinders with respect to the incident wave crest elevation $\eta_0 = 0.789$ m (η_{cyl1}/η_0

and η_{cyl2}/η_0). In the following sections, results from selected cases are presented to obtained detailed insights into the breaking wave interaction, free surface features and wave forces on the cylinders. The selected cases present the prominent breaking wave hydrodynamics for different separation distances in different wave impact scenarios.

Table 1: Details of the setups used in the different simulations

Case	H (m)	T (s)	S (m)	scenario	F_0 (N)	F_1/F_0	F_2/F_0	η_{cyl1}/η_0	η_{cyl2}/η_0
A1	1.30	4.00	1D	overturning wave crest impact on cylinder 1 just below wave crest level	14000	0.92	0.59	1.58	1.69
A2			2D			0.95	0.58	1.64	1.75
A3			3D			0.91	0.45	1.57	1.58
A4			4D			0.90	0.48	1.56	1.62
A5			5D			0.88	0.55	1.59	1.70
A6			6D			0.88	0.52	1.68	1.58
B1	1.30	4.00	1D	overturning wave crest impact on cylinder 1 at wave crest level	13400	0.74	0.58	1.76	1.71
B2			2D			0.93	0.85	1.70	1.72
B3			3D			0.61	0.80	1.75	1.58
B4			4D			0.75	0.57	1.69	1.56
B5			5D			0.83	0.61	1.69	1.45
B6			6D			0.86	0.60	1.70	1.37
C1	1.30	4.00	1D	wave breaking exactly at cylinder 1	11850	0.89	0.66	1.82	1.77
C2			2D			0.90	0.84	1.70	1.84
C3			3D			0.92	0.97	1.82	1.70
C4			4D			0.86	0.92	1.76	1.63
C5			5D			0.83	0.71	1.70	1.44
C6			6D			0.83	0.61	1.76	1.32
D1	1.30	4.00	1D	wave breaking just behind cylinder 1	9800	0.90	0.81	1.83	1.79
D2			2D			0.89	0.99	1.94	1.89
D3			3D			0.90	1.03	1.70	1.76
D4			4D			0.88	1.04	1.78	1.59
D5			5D			0.85	1.18	1.83	1.45
D6			6D			0.85	1.02	1.78	1.37

Scenario A1: overturning wave crest impacting cylinder 1 just below the wave crest level with $S = 1D$ The breaking wave force and free surface elevations around the cylinders calculated for scenario A1 are presented in Fig. (4). The breaking wave force on a single cylinder in this wave impact scenario is $F_0 = 14000$ N. The breaking wave forces (F) on cylinders 1 and 2 are calculated to be $0.92F_0$ and $0.59F_0$ respectively as shown in Fig. (4a). In this case, the incident wave on the second cylinder is a broken wave that has dissipated most of its energy during the breaking process and with the first cylinder. Thus, the breaking wave force on the second cylinder is significantly lower than that on the first cylinder. The free surface elevations (η) calculated in front of (WG 1) and behind (WG 2) the first cylinder and in front of the second cylinder (WG 3) are presented in Fig. (4b). The free surface elevation in front of cylinder 2, placed $S = 1D$ away is $\eta/\eta_0 = 1.69$, higher than the free surface elevation in front of cylinder 1, $\eta/\eta_0 = 1.58$. The higher free surface elevation is attributed to the large

runup on cylinder 2 due to the close placement of the cylinders.

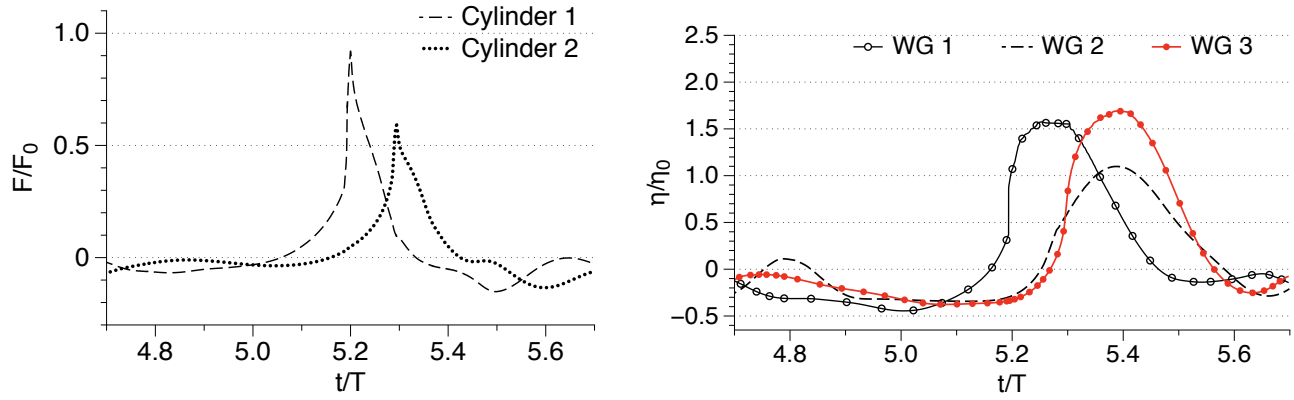

(a) breaking wave forces on the cylinders

(b) free surface elevations around the cylinders

Figure 4: Wave forces on and free surface elevations around the cylinders for scenario A1: breaker tongue impacting cylinder just below wave crest level with $S = 1D$

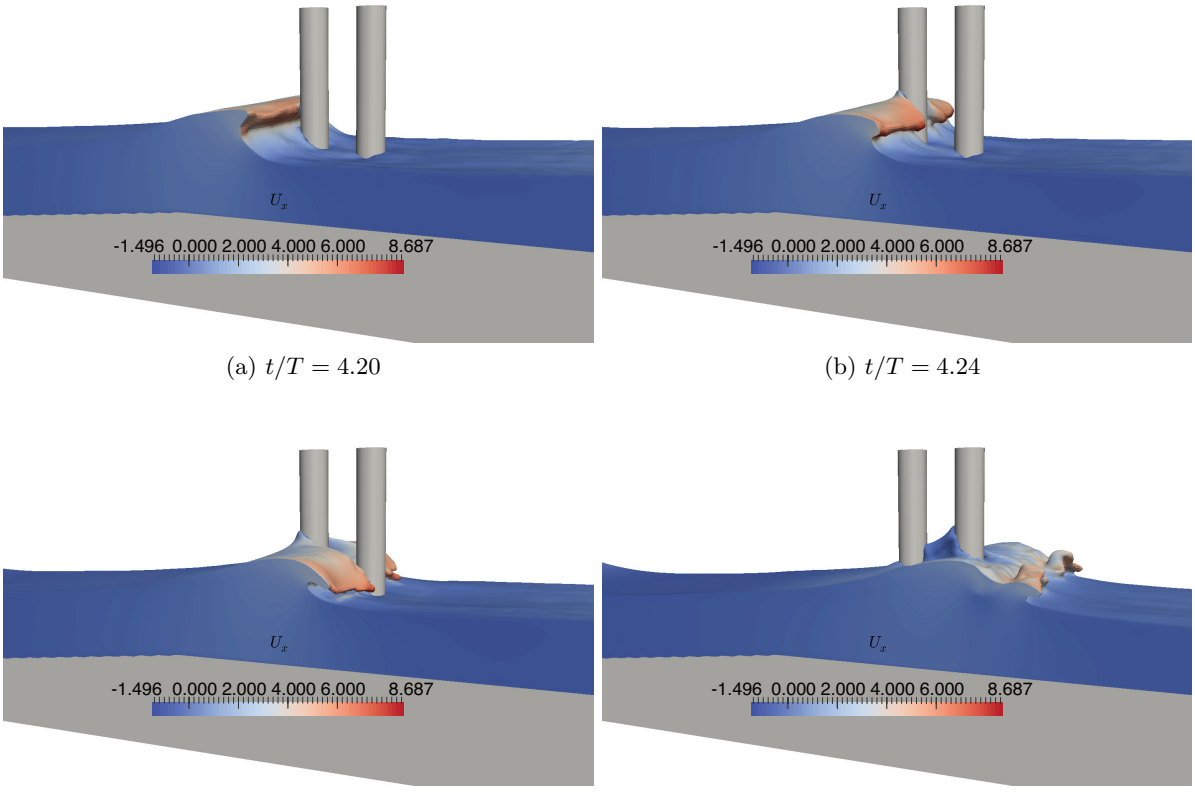

(a) $t/T = 4.20$

(b) $t/T = 4.24$

(c) $t/T = 4.29$

(d) $t/T = 4.40$

Figure 5: Free surface around the cylinders in scenario A1 ($S = 1D$) with horizontal velocity contours

Further insight into the wave interaction problem is obtained from the free surface around the cylinders for case A1, presented in Fig. (5) with horizontal velocity contours. The incident wave impacts cylinder 1 with the breaker tongue just below the wave crest level in Fig. (5a). The overturned wavefront is separated around cylinder 1 in Fig. (5b). This phenomenon of separation of the wave crest around the first cylinder and spreading of the water mass around the sides of the cylinder is also reported by Sparboom et al. (2006) in large-scale experiments. Figure (5c) shows how the separated broken wavefront incident on cylinder 2 reconnects with the free surface. As the broken wave crest propagates past cylinder 2 in Fig. (5d), high runup is observed on the front surface of cylinder 2. This runup results in a higher free surface elevation in front of cylinder 2 compared to cylinder 1 seen for WG 3 in Fig. (4b). Figure (5) also shows that in scenario A, cylinder 2 is always exposed to an already broken wave, which exerts lower wave forces on the cylinder.

Scenario B2: overturning wave crest impacting cylinder 1 at the wave crest level with $S = 2D$ Figure (6) shows the breaking wave forces on and the free surface elevations around the two cylinders in scenario B2. A single cylinder in the same impact scenario experiences a force of $F_0 = 13400$ N. The breaking wave force on cylinder 1 is $0.93F_0$, and on cylinder 2 it is $0.85F_0$, as shown in Fig.(6a). In Fig. (6b) the free surface elevations in front of cylinders 1 and 2 are $\eta/\eta_0 = 1.70$ and $\eta/\eta_0 = 1.72$ respectively. The slopes of the wavefront at the moment of impact on the cylinders are similar, and the wave forces on the two cylinders are comparably similar.

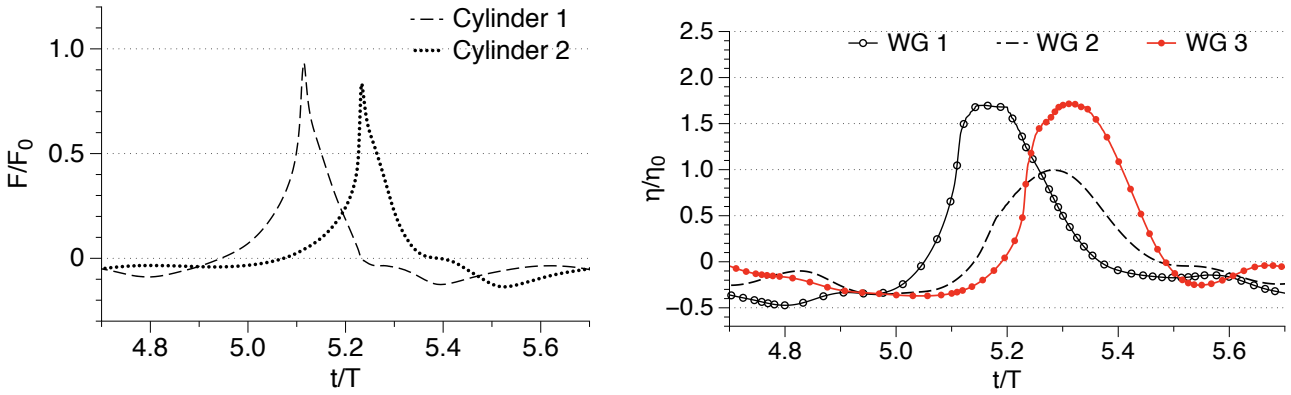

(a) breaking wave forces on the cylinders

(b) free surface elevations around the cylinders

Figure 6: Wave forces on and free surface elevations around the cylinders for scenario B2: breaker tongue impacting cylinder at wave crest level with $S = 2D$

Fig. (7) shows the free surface around the cylinders with horizontal velocity contours for scenario B2. The overturning wave crest impacts cylinder 1 at the wave crest level in Fig. (7a). The incident wave crest shows that it interacts with previous waves reflected off the cylinders. The separation of the overturning wave crest around cylinder 1 is seen in Fig. (7b). In Fig. (7c), the overturning wave crest and the water jet formed behind cylinder 1 impact cylinder 2 below the wave crest level. The high runup on the second cylinder due to the water jet originating behind cylinder 1 and the small separation distance is seen in Fig. (7d). In this scenario, although cylinder 1 separates the wavefront, the sheltering effect on cylinder 2

is seen to be reduced. This is due to the water jet that forms behind cylinder 1 and impacts cylinder 2 along with the breaking wave. This results in comparably similar forces on the two cylinders in this scenario, with the upstream cylinder experiencing a slightly higher force.

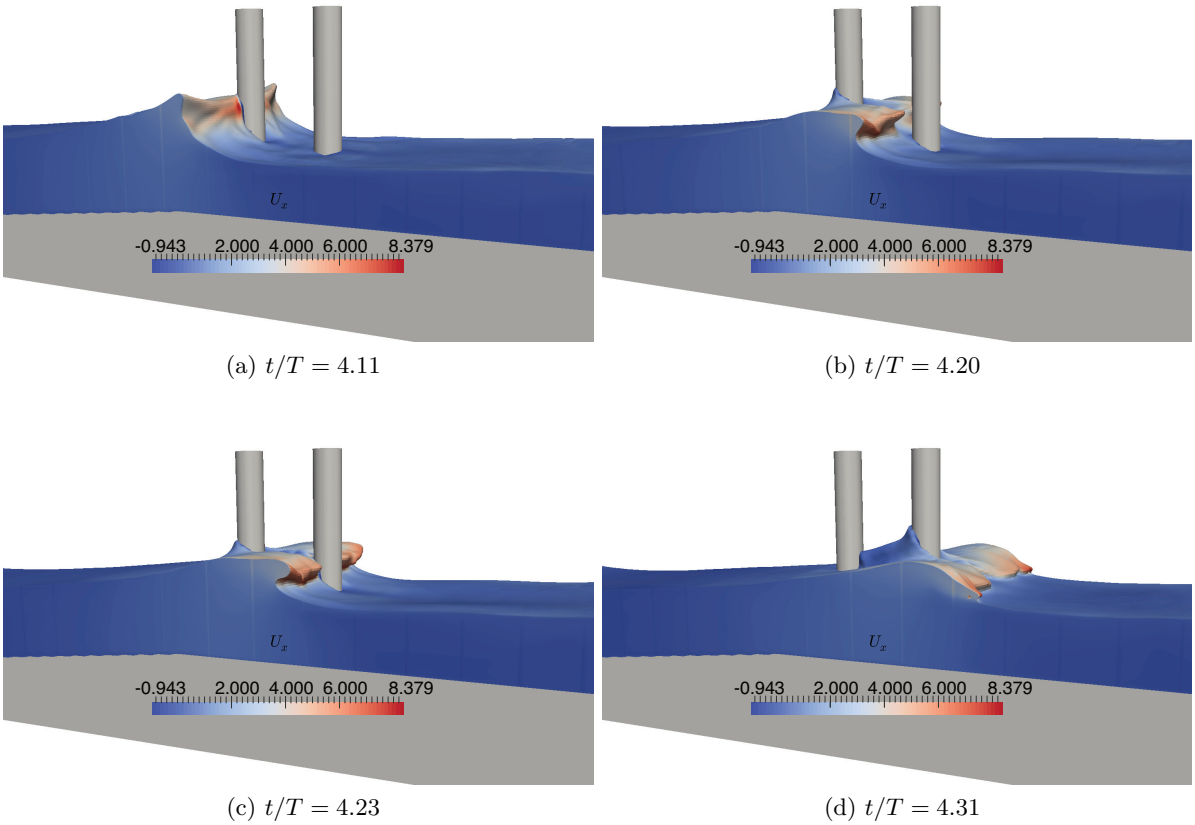

(a) $t/T = 4.11$ (b) $t/T = 4.20$

(c) $t/T = 4.23$ (d) $t/T = 4.31$

Figure 7: Free surface around the cylinders in scenario B2 ($S = 2D$) with horizontal velocity contours

Scenario C3: wave breaking exactly at cylinder 1 with $S = 3D$ The breaking wave forces on and the free surface elevations around the cylinders in scenario C3 are shown in Fig. (8). The breaking wave force on a single cylinder in this scenario is $F_0 = 11850$ N. Here, cylinder 1 experiences a force of $0.92F_0$ and cylinder 2 a force of $0.97F_0$. The breaking wave force on the downstream cylinder 2 is slightly higher than the force on the upstream cylinder 1. The free surface elevation in front of cylinder 2 is $\eta/\eta_0 = 1.70$, which is slightly lower when compared to $\eta/\eta_0 = 1.82$ in front of cylinder 1.

The wave interaction in scenario C3 is further studied using the free surface around the cylinders and horizontal velocity contours shown in Fig. (9). The incident wave impacts cylinder 1 with a vertical wavefront as seen in Fig. (9a). The incident wave separates around cylinder 1 in Fig. (9b), and the wave crest also begins to overturn just behind the cylinder. The breaker tongue and the water jet originating behind cylinder 1 impact cylinder 2 in Fig. (9c). The breaking wave incident on cylinder 2 impacts the cylinder just below the wave

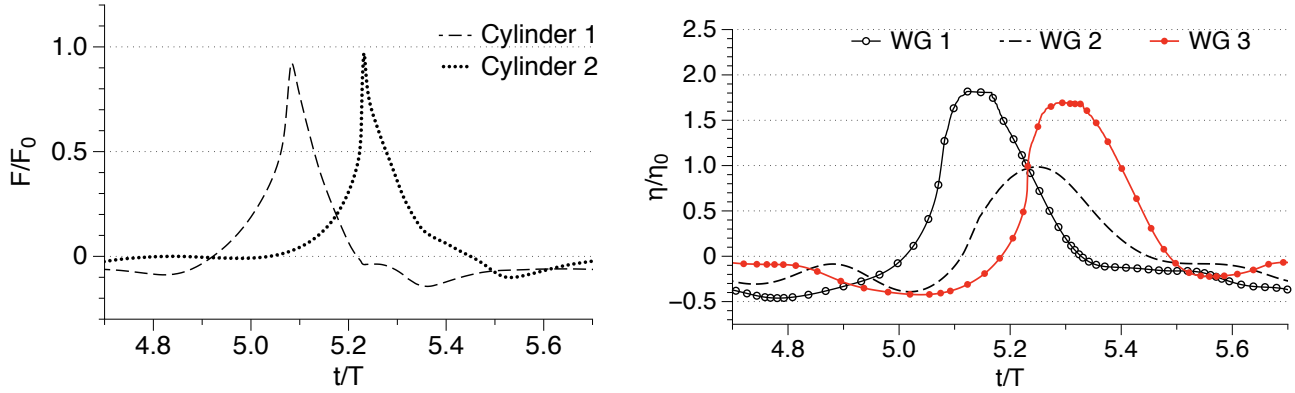

(a) breaking wave forces on the cylinders

(b) free surface elevations around the cylinders

Figure 8: Wave forces on and free surface elevations around the cylinders for scenario C3: wave breaking exactly at the first cylinder with $S = 3D$

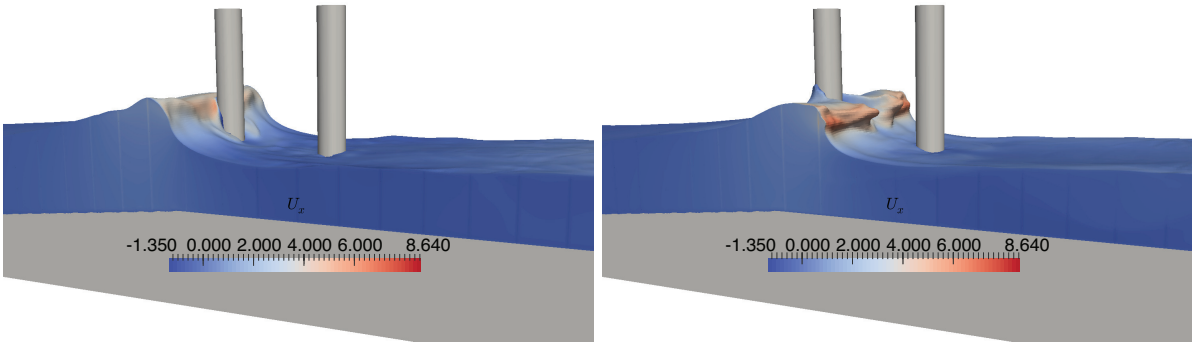

(a) $t/T = 4.08$

(b) $t/T = 4.18$

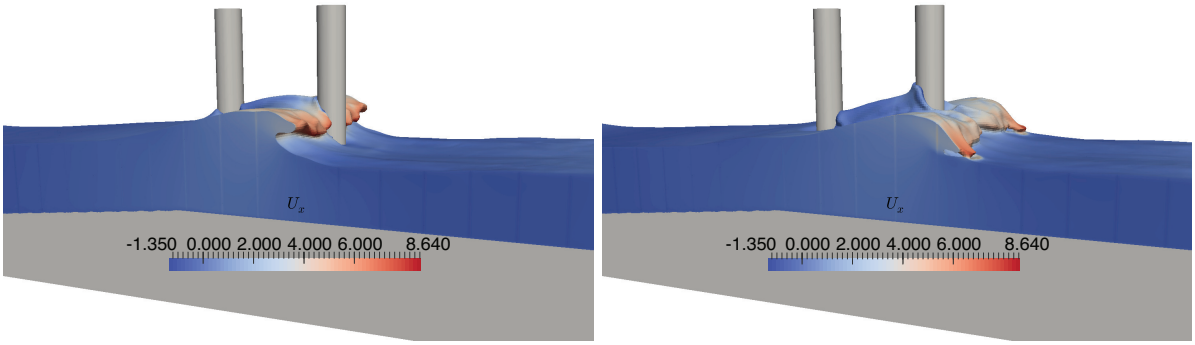

(c) $t/T = 4.25$

(d) $t/T = 4.32$

Figure 9: Free surface around the cylinders in scenario C3 ($S = 3D$) with horizontal velocity contours

crest level; this breaking wave and the water jet result in higher forces on the cylinder. The

runup of the trapped water between the cylinders is seen in Fig. (9d), and the overturning wave crest rejoins the preceding wave crest after passing cylinder 2.

Scenario D4: wave breaking just behind cylinder 1 with $S = 4D$ The waves force on a single cylinder in this wave impact scenario is calculated to be $F_0 = 9800$ N. In Fig. (10a), the calculated breaking wave forces on cylinders 1 and 2 are $0.88F_0$ and $1.04F_0$ respectively. In this scenario, the upstream cylinder 1 is exposed to very steep incident waves that approach the wave breaking point. Cylinder 2 is exposed to an overturning wave crest, and the breaking wave impact force contributes to the total wave force on the cylinder; this results in a higher wave force on the downstream cylinder compared to the upstream cylinder. The free surface elevations in Fig. (10b) show that $\eta/\eta_0 = 1.78$ in front of cylinder 1 (WG 1) and that $\eta/\eta_0 = 1.59$ in front of cylinder 2 (WG 3) for this case.

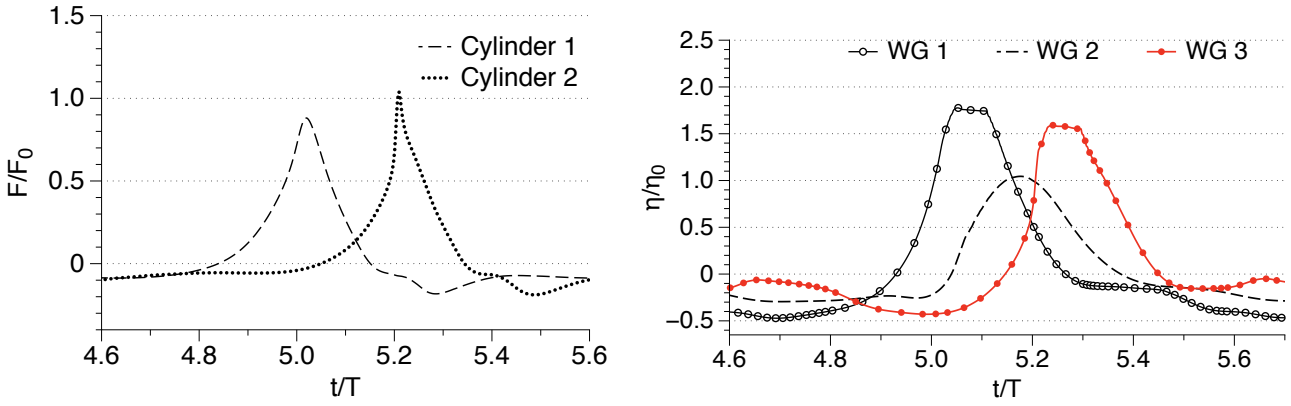

(a) breaking wave forces on the cylinders

(b) free surface elevations around the cylinders

Figure 10: Wave forces on and free surface elevations around the cylinders for scenario D4: wave breaking just behind the first cylinder with $S = 4D$

To further understand the wave interaction with the cylinders in scenario D4, the free surface around the cylinders is presented in Fig. (11) along with the horizontal velocity contours. Figure (11a) shows the steep unbroken wave incident on cylinder 1. The wave breaks just behind cylinder 1; the overturning wave crest, along with the water jet originating behind cylinder 1, is seen in Fig. (11b). The overturning wave crest and the water jet then impact the second cylinder just below the wave crest level in Fig. (11c). The breaker tongue reconnects with the preceding wave trough behind cylinder 2 in Fig. (11d). The higher forces on the second cylinder result from the mode of wave impact on each cylinder. Figure (11) clearly shows that the upstream cylinder 1 is exposed to a steep non-breaking wave, whereas the overturning wave crest impacts the downstream cylinder 2 just below the wave crest level.

Scenario D6: wave breaking just behind cylinder 1 with $S = 6D$ The wave forces on cylinders 1 and 2 for this case are calculated to be $0.85F_0$ and $1.03F_0$ respectively as shown in Fig. (12a). The wave force on cylinder 2 is significantly higher than the force on cylinder 1 in this scenario. The free surface elevation in front of cylinder 1, $\eta/\eta_0 = 1.78$, is higher than the free surface in front of cylinder 2, which is $\eta/\eta_0 = 1.37$ in Fig. (12b). The runup on cylinder 2 is less for this scenario ($\eta/\eta_0 = 1.37$) when compared to scenario D4 ($\eta/\eta_0 = 1.59$).

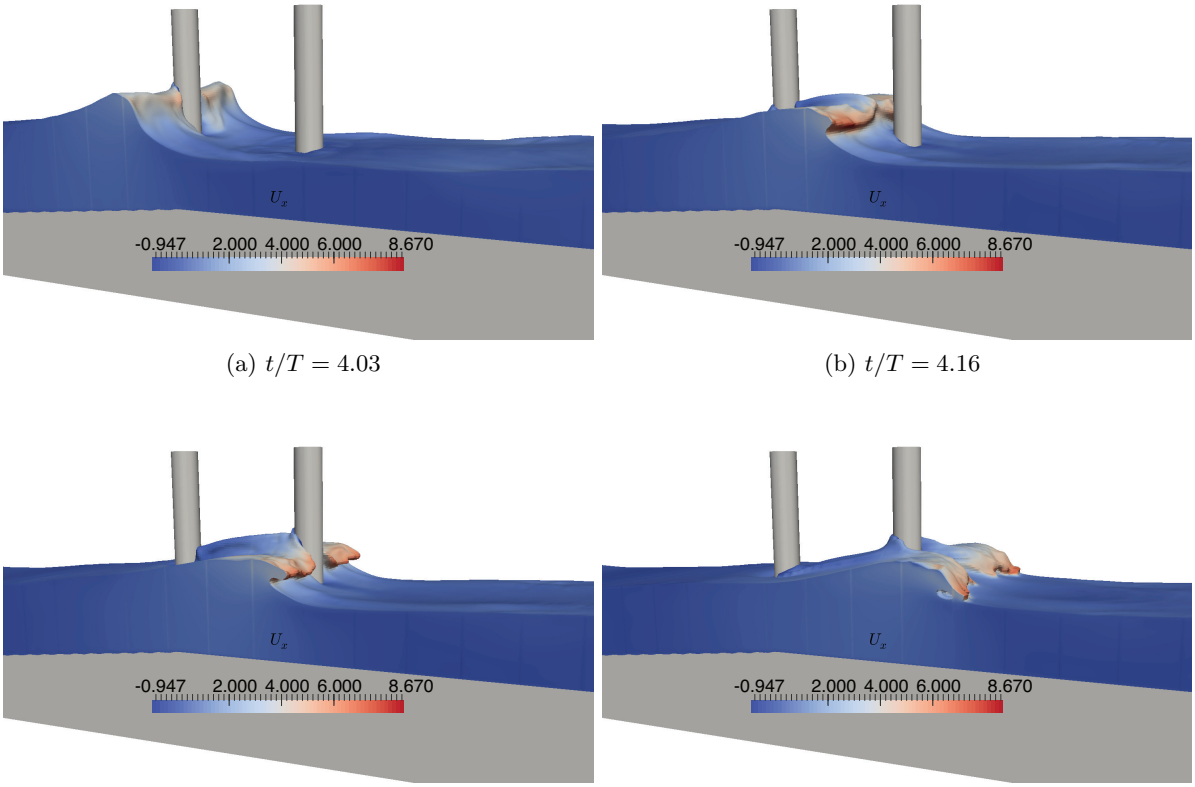

(a) $t/T = 4.03$ (b) $t/T = 4.16$

(c) $t/T = 4.21$ (d) $t/T = 4.30$

Figure 11: Free surface around the cylinders in scenario D4 ($S = 4D$) with horizontal velocity contours

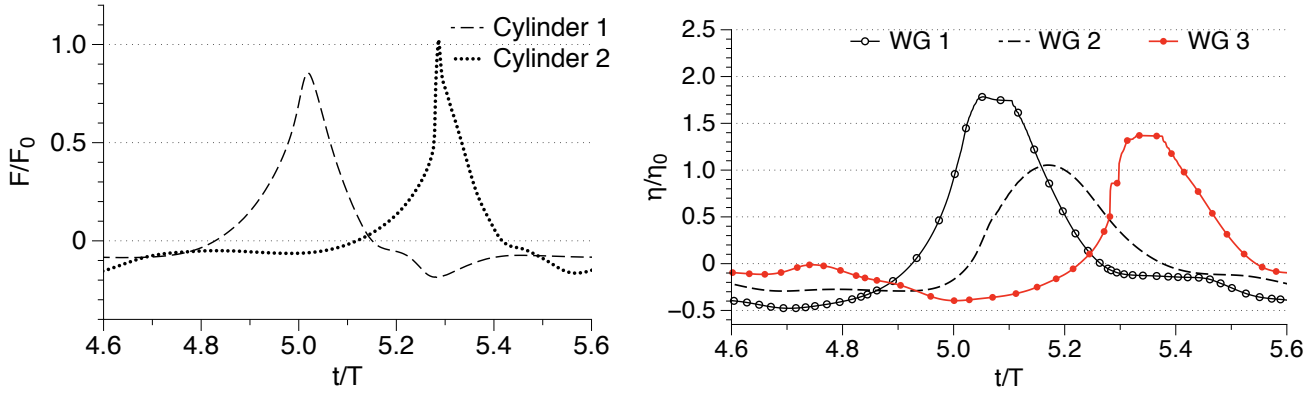

(a) breaking wave forces on the cylinders (b) free surface elevations around the cylinders

Figure 12: Wave forces on and free surface elevations around the cylinders for scenario D6: wave breaking just behind the first cylinder with $S = 6D$

The free surface around the cylinders and the horizontal velocity contours are presented in

Fig. (13). The steep unbroken wave incident on cylinder 1 is seen in Fig. (13a), similar to that in Fig. (11a). Figure (13b) shows the overturning crest and the water jet originating behind cylinder 1 in between the two cylinders. Fig. (13c) shows the water jet impact on cylinder 2 after the overturning wave crest has impacted the cylinder is seen in . The runup on cylinder 2 in this scenario is lower due to the longer separation distance between the cylinders. The overturning wave crest and the water jet impact the cylinder close to the point where the breaking wave crest reconnects with the preceding wave trough. The broken wave and the water jet formed behind cylinder 2 are seen in Fig. (13d).

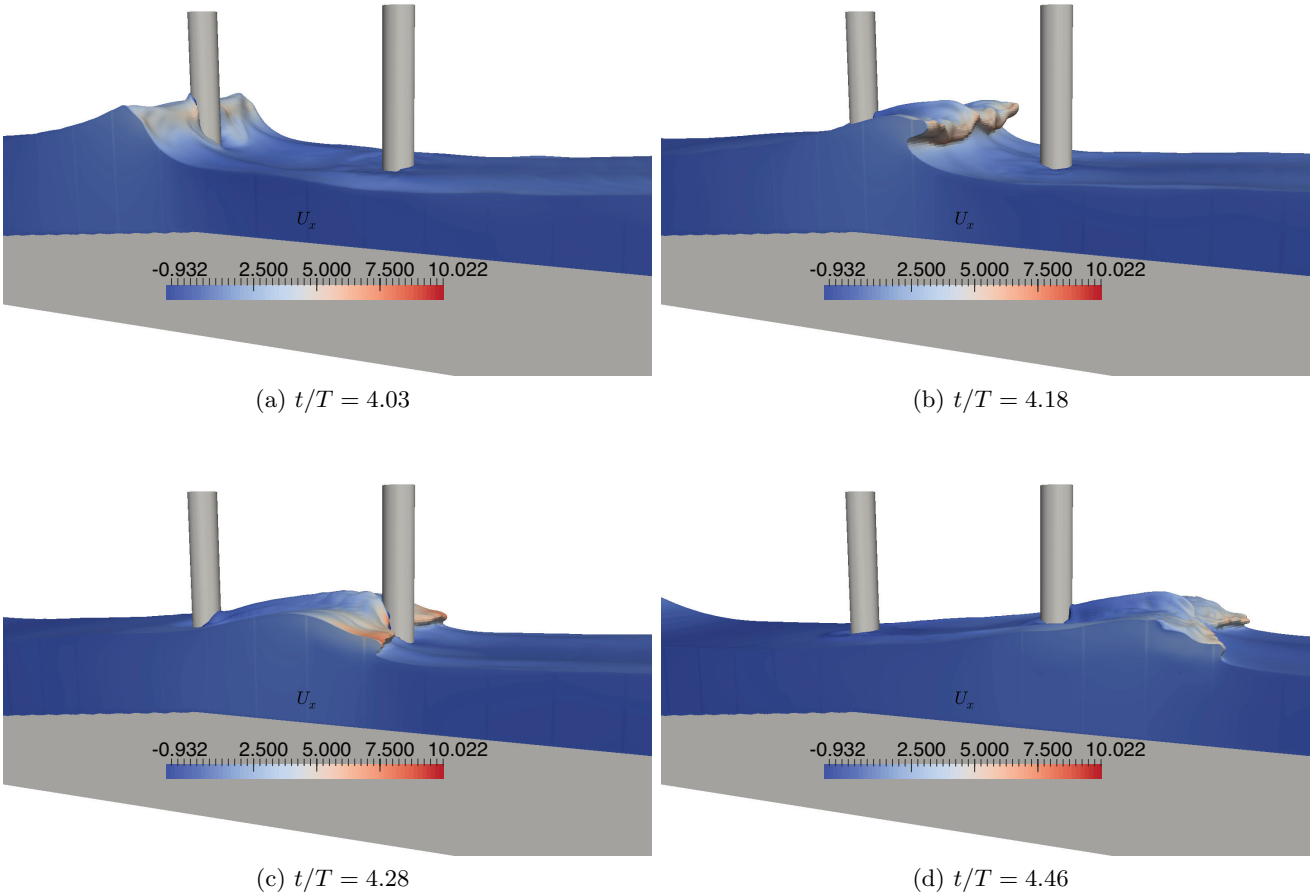

(a) $t/T = 4.03$ (b) $t/T = 4.18$

(c) $t/T = 4.28$ (d) $t/T = 4.46$

Figure 13: Free surface around the cylinders in scenario D6 ($S = 6D$) with horizontal velocity contours

3.3 Variation of the breaking wave forces with separation distance in the different wave impact scenarios

The variation of the total breaking wave forces on each of the cylinders in the different wave impact scenarios and separation distances is presented in Fig. (14). The following sections correlate the variation of the forces with the separation distance with the free surface features associated with the wave impact scenario.

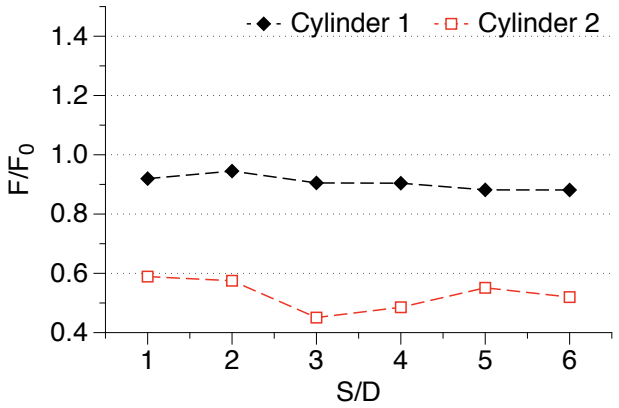

(a) scenario A: breaker tongue impact on cylinder 1 just below wave crest level

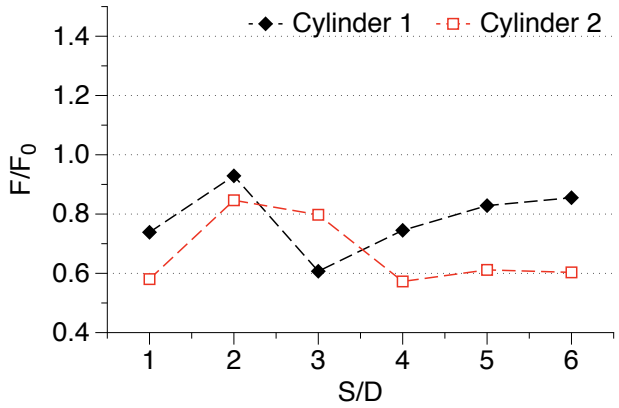

(b) scenario B: breaker tongue impact on cylinder 1 at wave crest level

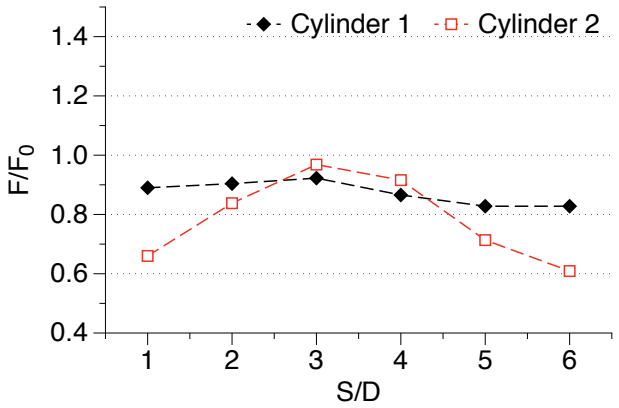

(c) scenario C: wave breaking exactly at cylinder 1

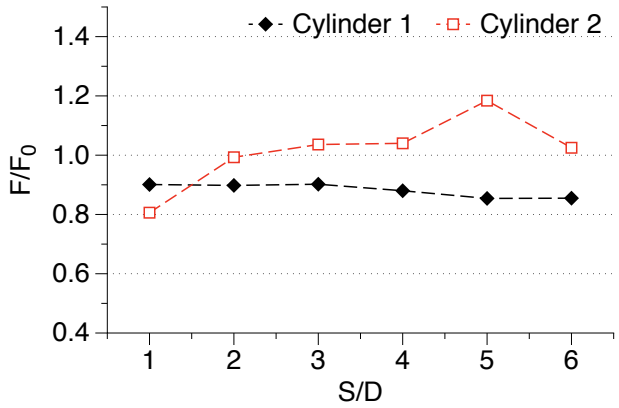

(d) scenario D: wave breaking just behind cylinder 1

Figure 14: Variation of the maximum wave force on the cylinders with distance of separation S in different wave impact scenarios

Scenario A The total wave force on cylinder 1 varies over a small range, between $0.95F_0$-$0.88F_0$ for scenario A in Fig. (14a). For cylinder 2, the total wave force varies significantly with a lowest value of $0.45F_0$ when $S = 3D$ to a highest value of $0.59F_0$ when $S = 1D$. Cylinder 2 is always exposed to a broken wave and the water jet originating behind cylinder 1; the free surface features behind cylinder 1 have a significant effect on the total wave force on cylinder 2. For small separation distances of $S = 1D$ and $2D$, a separated broken wave crest is incident on cylinder 2, as seen in Fig. (5c). The water jet originating behind cylinder 1, which develops in the small region between the cylinders, is mainly responsible for the force on cylinder 2. The resulting forces for $S = 1D$ and $2D$ are seen to be around $0.58F_0$ in Fig. (14a). When the separation distance increases to $S = 3D$, the force resulting from the impact of the water jet is reduced, and the minimum force is calculated for this scenario. On further increasing the separation distance to $S = 4D$ and $5D$, the wave crest separated by cylinder 1 rejoins the preceding wave trough, undergoes secondary breaking and impacts

cylinder 2 along with the water jet. This results in a slight increase in the force on cylinder 2. For $S = 6D$, cylinder 2 is mainly exposed to the post-breaking splash up, and the force on cylinder 2 decreases. Further increases in the separation distance S would result in further reductions in the wave force on cylinder 2.

Scenario B The total wave forces on both cylinders are significantly affected by the separation distances between the cylinders in this scenario, as seen in Fig. (14b). The total wave force on cylinder 1 is highest for $S = 2D$ with a value of $0.93F_0$ and lowest for $S = 3D$ with a value of $0.61F_0$. For cylinder 2, the total wave force has a maximum value of $0.85F_0$ for $S = 2D$, and a minimum value of $0.57F_0$ for $S = 4D$. For this case, the waves reflected from the cylinders interact with the incident overturning wave crest as seen in Fig. (7a). This results in significant changes in wave forces on both cylinders as the separation distance between the cylinders is varied. When $S = 1D$, the incident wave is separated by cylinder 1, and cylinder 2 is impacted mainly by the water jet. This results in lower forces on cylinder 2. As S increases to $2D$, the separated wave crest rejoins just before impacting cylinder 2, and the force on the cylinder increases. The interaction between the incident wave crest and the reflected waves from the cylinders for $S = 3D$ results in reduced forces on cylinder 1. At the same time, the wave incident on cylinder 2 rejoins the preceding wave trough just in front of the cylinder. The force on the cylinder is reduced, but it is higher than the force on cylinder 1. Further increases in S result in lower forces on cylinder 2, since the incident wave has rejoined the preceding wave trough and the cylinder is exposed to splash up. The forces on cylinder 1 increase and nearly reach the value calculated for $S = 1D$ following the interaction between the incident and reflected waves. Hildebrandt et al. (2008) found through large-scale experiments with non-breaking waves on groups of slender cylinders that for certain distances of separation, the forces on the upstream cylinder are influenced by the wave interaction between the cylinders and waves reflected by the cylinders. Their observations are applicable in this case with a strong interaction between the incident wave and the reflected waves when the overturning wave crest impacts cylinder 1 at wave crest level.

Scenario C In scenario C the front surface of cylinder 1 is at the wave breaking point, and the peak breaking wave force on the cylinder varies between $0.92F_0$ ($S = 3D$) and $0.83F_0$ ($S = 6D$) in Fig. (14c). The peak wave force on cylinder 2 varies significantly with the separation distance, with a maximum of $0.97F_0$ for $S = 3D$ and a minimum of $S = 0.61F_0$ for $S = 6D$. When $S = 3D$ and $4D$, the breaking wave force on downstream cylinder 2 is slightly higher than on upstream cylinder 1. In this scenario, the variation in the forces on cylinder 2 can be attributed to the wave breaking process and the resulting free surface features seen between the cylinders. For $S = 1D$, the incident wave is separated by cylinder 1, and the water jet originating behind the cylinder impacts cylinder 2, leading to a lower force on the cylinder. The separated wave crest rejoins before impacting cylinder 2; this impact and the water jet increases the wave force when $S = 2D$. On further increasing S to $3D$ and $4D$, the breaker tongue impacts the cylinder around the wave crest level along with the water jet as seen in Fig. (9c), resulting in a higher force on cylinder 2 than on cylinder 1. For $S = 5D$ and $6D$, cylinder 2 is exposed mainly to the splash up along with the water jet. The impact of the broken wave on cylinder 2 results in a lower force for $S = 5D$ and $6D$; further increases in S would result in a lower force.

Scenario D The total wave force on cylinder 1 in scenario D varies over a small range between $0.84F_0$-$0.90F_0$ in Fig. (14d). The peak wave force on cylinder 2 is the lowest for $S = 1D$ ($0.81F_0$) and the highest for $S = 5D$ ($1.18F_0$). Due to the wave breaking just behind the upstream cylinder 1, cylinder 2 is exposed to breaking wave impact and generally experiences higher forces than cylinder 1. Similar to the previous scenarios where cylinder 2 is placed at a distance of $S = 1D$, the incident wave crest is separated by cylinder 1, resulting in a lower wave force on cylinder 2. From $S = 2D$ to $S = 5D$, cylinder 2 is impacted by the overturning wave crest at and around the wave crest level as seen in Fig. (11c) when $S = 4D$, leading to higher wave forces. The maximum peak force is calculated when $S = 5D$, where the breaker tongue impacts cylinder 2 just below the wave crest level. On increasing S to $6D$, the overturning wave crest rejoins the preceding wave trough during impact with cylinder 2 as seen in Fig. (13c); the wave force on cylinder 2 is reduced.

3.4 Discussion

The results show that the wave forces on both cylinders are generally less than the wave force on a single cylinder in the same wave impact scenario (F_0). The exception to this observation are the cases where the breaker tongue impacts the downstream cylinder 2 around the wave crest level. This is particularly the case in scenario D, where the wave breaks behind the upstream cylinder 1 and the overturning wave crest impacts cylinder 2 at or just below wave crest level depending on the separation distance between the cylinders. Another observation is that high runups are calculated on the second cylinder when the cylinders are placed close to each other ($S = 1D$ or $2D$), but the higher free surface elevations do not correspond to higher wave forces. In fact, for scenarios C3, D4 and D6 the free surface in front of cylinder 2 is lower than that in front of cylinder 1 whereas wave forces are higher on cylinder 2. The close placement of the cylinders leads to a high runup from the water jet developed in the region between the cylinders, but the second cylinder is shielded from breaking wave impact due to the separation of the incident wavefront by the first cylinder.

The trend of the breaking wave forces on cylinder 1 for scenario B varies greatly from the trend seen in the other scenarios for $S = 2D$ and $3D$. This is due to the strong interaction between the incident waves and the waves reflected from the cylinder, as seen in previous studies by Hildebrandt et al. (2008) for cylinders placed close together. In addition, the superposition of the reflected waves on the overturning wave crest is the strongest as seen from Fig. (7a). This leads to a large increase followed by a large decrease in the breaking wave forces for $S = 2D$ and $S = 3D$, respectively, in this scenario. On further increase in S, the breaking wave forces on cylinder 1 are around the values obtained for $S = 1D$, which is the general trend in all the other scenarios.

Some similarities can be drawn between the results for wave forces on tandem cylinders in this study and results for breaking wave forces on a single cylinder in previous studies. With a single cylinder, the maximum wave forces are obtained when the breaker tongue impacts the cylinder just below the wave crest level (Irschik et al., 2002). In the present study, the upstream cylinder 1 also experiences the highest forces in scenario A2 ($F = 13300N$), when the breaking wave impacts the cylinder just below wave crest level. In scenario D4, cylinder 1 experiences one of the lowest forces ($F = 8330N$) when the wave breaks just behind the cylinder. However, the lowest force on cylinder 1 is calculated in scenario B3 ($F = 8174N$) when the overturning wave crest impacts cylinder 1 at the wave crest level. This is due to the

interaction between the incident and reflected waves.

For cylinder 2, the highest forces are calculated in scenario D5 ($F = 11564N$), when the cylinder is placed at $S = 5D$ from cylinder 1, and the wave breaks just behind cylinder 1. The overturning wave crest impacts cylinder 2 just below the wave crest level along with the water jet. This is similar to the wave impact scenario leading to the highest breaking wave force on a single cylinder. The lowest force on cylinder 2 ($F = 6300N$) is calculated in scenario A3, where the overturning wave crest rejoins the preceding wave trough before impact with the cylinder. Thus, the results for breaking wave impact on a single slender cylinder by Wienke et al. (2000) and Irschik et al. (2002) are applicable to the case of tandem cylinders as well, though with a few changes due to the interaction between the two cylinders placed in proximity. The results in this study differ from the small-scale experimental results presented by Apelt and Piorewicz (1986), which concluded that the separation between the cylinders did not affect the wave forces on the cylinders when they are arranged in the direction of wave propagation.

4 Conclusions

The open-source CFD model REEF3D is used to simulate plunging breaking wave interaction with a pair of cylinders placed in tandem at different separation distances for different wave impact scenarios. The model was validated by comparing the numerical results for wave forces and free surface elevations with the experimental results for breaking waves on a single cylinder at the Large Wave Flume in Hannover, Germany by Irschik et al. (2002). The free surface features associated with breaking wave interaction with a slender cylinder are presented and correlated to the wave forces on the cylinders, and the following conclusions can be drawn from the results:

- Similar to the results for wave impact on a single slender cylinder, the maximum breaking wave forces in this study is calculated for cases where the breaker tongue impacts the cylinder just below the wave crest level.

- The free surface features behind the first cylinder, such as the separation of the wavefront around the first cylinder, the formation of a water jet, the rejoining of the separated wavefront and the reconnection of the overturning wave crest with the preceding wave trough, have significant influence on the wave forces on the second cylinder. The distance between the cylinders also determines the development of the various free surface features.

- The wave forces on the first cylinder are less than the forces on a single cylinder for the same wave impact scenario for all the cases studied. The highest force on the first cylinder is $0.95F_0$ when the wave impacts the cylinder just below the wave crest level and the second cylinder is at a distance of $2D$.

- The wave forces on the second cylinder are generally lower than the forces on the first cylinder when the wave breaks in front of or on the first cylinder and the separation distance is more than $4D$, with a highest force of $0.71F_0$ when the wave breaks exactly at the first cylinder.

- The wave force on the second cylinder is higher than both the force on the first cylinder and the force on a single cylinder when the breaker tongue impacts the second cylinder around the wave crest level. The highest force on the second cylinder is $1.18F_0$ when the wave breaks just behind the first cylinder and the second cylinder is at a distance of $5D$.

This study provides insight into the challenging problem of plunging breaking wave interaction with two cylinders in tandem for different wave impact scenarios and distances of separation. Further studies can be carried out and extended to investigate breaking wave interaction with three or more cylinders in tandem, including oblique wave incidence to represent engineering problems including tripod substructures and coastal constructions with multiple cylinders in proximity.

5 Acknowledgements

This study has been carried out under the OWCBW project (No. 217622/E20) and the authors are grateful to the grants provided by the Research Council of Norway. This research was supported in part with computational resources at the Norwegian University of Science and Technology (NTNU) provided by NOTUR, http://www.notur.no (NN2620K).

References

Alagan Chella, M., Bihs, H. and Myrhaug, D. (2015*a*). Characteristics and profile asymmetry properties of waves breaking over an impermeable submerged reef. *Coastal Engineering*, **100**, 26–36.

Alagan Chella, M., Bihs, H., Myrhaug, D. and Muskulus, M. (2015*b*). Breaking characteristics and geometric properties of spilling breakers over slopes. *Coastal Engineering*, **95**, 4–19.

Alagan Chella, M., Tørum, A. and Myrhaug, D. (2012). An overview of wave impact forces on offshore wind turbine substructures. *Energy Procedia*, **20**, 217–226.

Apelt, C.J. and Piorewicz, J. (1986). Interference effects on breaking wave forces on rows of vertical cylinders. In: *Proc. 1st Australasian Port, Harbour and Offshore Engineering Conference, Sydney, Australia.*

Arntsen, Ø.A., Ros, X. and Tørum, A. (2011). Impact forces on a vertical pile from plunging breaking waves. In: *Coastal Structures.*

Battjes, J.A. and Sakai, T. (1981). Velocity field in a steady breaker. *Journal of Fluid Mechanics*, **111**, 421–437.

Berthelsen, P.A. and Faltinsen, O.M. (2008). A local directional ghost cell approach for incompressible viscous flow problems with irregular boundaries. *Journal of Computational Physics*, **227**, 4354–4397.

Blenkinsopp, C.E. and Chaplin, J.R. (2008). The effect of crest submergence on wave breaking over submerged slopes. *Coastal Engineering*, **55**, 967–974.

Bonmarin, P. (1989). Geometric properties of deep-water breaking waves. *Journal of Fluid Mechanics*, **209**, 405–433.

Bradford, S.F. (2000). Numerical simulation of surf zone dynamics. *Journal of Waterway, Port, Coastal and Ocean Enginnering*, **126**, 1–13.

Bredmose, H. and Jacobsen, N.G. (2010). Breaking wave impacts on offshore wind turbine foundations: focused wave groups and CFD. *Proc., 29th International Conference on Ocean, Offshore and Arctic Engineering, Shanghai, China.*

Chan, E.S. and Melville, W.K. (1988). Deep-water plunging wave pressures on a vertical plane wall. In: *Proc. of the Royal Society of London. A. Mathematical and Physical Sciences*, volume 417, 95–131.

Chaplin, J.and Flintham, T., Greated, C. and Skyner, D. (1992). Breaking wave forces on a vertical cylinder. Technical report, Health and Safety Executive, London, UK.

Chen, G., Kharif, C., Zaleski, S. and Li, J. (1999). Two-dimensional Navier-Stokes simulation of breaking waves. *Physics of Fluids*, **11**, 121–133.

Choi, S.J., Lee, K.H. and Gudmestad, O.T. (2015). The effect of dynamic amplification due to a structure s vibration on breaking wave impact. *Ocean Engineering*, **96**, 8–20.

Chorin, A. (1968). Numerical solution of the Navier-Stokes equations. *Mathematics of Computation*, **22**, 745–762.

Christensen, E.D. (1998). Turbulence in breaking waves – a numerical investigation. PhD thesis.

Christensen, E.D. (2006). Large eddy simulation of spilling and plunging breakers. *Coastal Engineering*, **53**(5–6), 463–485.

Christensen, E.D. and Deigaard, R. (2001). Large eddy simulation of breaking waves. *Coastal Engineering*, **42**, 53–86.

Cokelet, E.D. (1977). Breaking waves. *Nature*, **267**, 769–774.

Duncan, J.H. (2001). Spilling breakers. *Annual Review of Fluid Mechanics*, **33**, 519–547.

Durbin, P.A. (2009). Limiters and wall treatments in applied turbulence modeling. *Fluid Dynamics Research*, **41**, 1–18.

Goda, Y., Haranaka, S. and Kitahata, M. (1966). Study on impulsive breaking wave forces on piles. *Report Port and Harbour Technical Research Institute*, **6**(5), 1–30.

Gourlay, M.R. (1994). Wave transformation on a coral reef. *Coastal Engineering*, **23**, 17–42.

Hieu, P.D., Katsutoshi, T. and Ca, V.T. (2004). Numerical simulation of breaking waves using a two-phase flow model. *Applied Mathematical Modeling*, **28**(11), 983–1005.

Higuera, P., Lara, L.J. and Losada, I.J. (2013). Realistic wave generation and active wave absorption for Navier-Stokes models application to OpenFOAM. *Coastal Engineering*, **71**, 102–118.

Hildebrandt, A. and Schlurmann, T. (2012). Breaking wave kinematics, local pressures, and forces on a tripod structure. In: *Coastal Engineering*, volume 1, 71.

Hildebrandt, A., Sparboom, U. and Oumeraci, H. (2008). Wave forces on groups of slender cylinders in comparison to an isolated cylinder due to non-breaking waves. In: *Coastal Engineering*, 3770–3781.

Irschik, K., Sparboom, U. and Oumeraci, H. (2002). Breaking wave characteristics for the loading of a slender pile. In: *Proc. 28th International Conference on Coastal Engineering, Cardiff, Wales*.

Jacobsen, N.G., Fuhrman, D.R. and Fredsøe, J. (2012). A wave generation toolbox for the open-source CFD library: OpenFOAM. *International Journal for Numerical Methods in Fluids*, **70**(9), 1073–1088.

Jiang, G.S. and Peng, D. (2000). Weighted ENO schemes for Hamilton-Jacobi equations. *SIAM Journal on Scientific Computing*, **21**, 2126–2143.

Jiang, G.S. and Shu, C.W. (1996). Efficient implementation of weighted ENO schemes. *Journal of Computational Physics*, **126**, 202–228.

Kamath, A., Alagan Chella, M., Bihs, H. and Arntsen, Ø.A. (2015). Cfd investigations of wave interaction with a pair of large tandem cylinders. *Ocean Engineering*, **108**, 738–748.

Kjeldsen, S. and Myrhaug, D. (1978). *Kinematics and dynamics of breaking waves*. River and Harbour Laboratory (NHL) The Norwegian Institute of Technology.

Larsen, J. and Dancy, H. (1983). Open boundaries in short wave simulations - a new approach. *Coastal Engineering*, **7**, 285–297.

Lin, P. and Liu, P.L.F. (1998). A numerical study of breaking waves in the surf zone. *Journal of Fluid Mechanics*, **359**, 239–264.

Miller, R.L. (1987). Role of vortices in surf zone prediction: sedimentation and wave forces. *The Society of Economic Paleontologists and Mineralogists, Special Publications*, (24), 92–114.

Mo, W., Jensen, A. and Liu, P.L.F. (2013). Plunging solitary wave and its interaction with a slender cylinder on a sloping beach. *Ocean Engineering*, **74**, 48–60.

Morison, J.R., O'Brien, M.P., Johnson, J.W. and Schaaf, S.A. (1950). Force exerted by surface waves on piles. *Journal of Petroleum Technology*, **2**, 149–154.

Nadaoka, K., Hino, M. and Koyano, Y. (1989). Structure of the turbulent flow field under breaking waves in the surf zone. *Journal of Fluid Mechanics*, **204**, 359–387.

Naot, D. and Rodi, W. (1982). Calculation of secondary currents in channel flow. *Journal of the Hydraulic Division, ASCE*, **108**(8), 948–968.

Osher, S. and Sethian, J.A. (1988). Fronts propagating with curvature- dependent speed: algorithms based on Hamilton-Jacobi formulations. *Journal of Computational Physics*, **79**, 12–49.

Peng, D., Merriman, B., Osher, S., Zhao, H. and Kang, M. (1999). A PDE-based fast local level set method. *Journal of Computational Physics*, **155**, 410–438.

Rapp, R.J. and Melville, W.K. (1990). Laboratory measurements of deep-water breaking waves. *Philosophical Transactions of the Royal Society of London A: Mathematical, Physical and Engineering Sciences*, **331**(1622), 735–800.

Sawaragi, T. and Nochino, M. (1984). Impact forces of nearly breaking waves on a vertical circular cylinder. *Coastal Engineering in Japan*, **27**, 249–263.

Schäffer, H.A. and Klopman, G. (2000). Review of multidirectional active wave absorption methods. *Journal of Waterway, Port, Coastal, and Ocean Engineering*, **126**(2), 88–97.

Shu, C.W. and Osher, S. (1988). Efficient implementation of essentially non-oscillatory shock capturing schemes. *Journal of Computational Physics*, **77**, 439–471.

Smith, E.R. and Kraus, N.C. (1990). Laboratory study on macro-features of wave breaking over bars and artificial reefs. Technical report, Coastal Engineering Research Center.

Sparboom, U., Hildebrandt, A. and Oumeraci, H. (2006). Group interaction effects of slender cylinders under wave attack. *Coastal Engineering*, 4430–4442.

Sparboom, U., Oumeraci, H., Schmidt-Koppenhagen, R. and Grüne, J. (2005). Large-scale model study on cylinder groups subject to breaking and nonbreaking waves. In: *Proc. 5th International Symposium WAVES 2005 Ocean Waves Measurement and Analysis, Madrid, Spain.*

Stive, M.J.F. and Wind, H.G. (1982). A study of radiation stress and set-up in the nearshore region. *Coastal Engineering*, **6**, 1–26.

Ting, F.C.K. and Kim, Y.K. (1994). Vortex generation in water waves propagating over a submerged obstacle. *Coastal Engineering*, **24**(1), 23–49.

van der Vorst, H. (1992). BiCGStab: A fast and smoothly converging variant of Bi-CG for the solution of nonsymmetric linear systems. *SIAM Journal on Scientific and Statistical Computing*, **13**, 631–644.

Wang, Z., Zou, Q. and Reeve, D. (2009). Simulation of spilling breaking waves using a two phase flow CFD model. *Computers and Fluids*, **38**(10), 1995–2005.

Watanabe, A. and Horikawa, K. (1974). Breaking wave forces on a large diameter cell. *Coastal Engineering Proceedings*, **1**(14).

Wienke, J. and Oumeraci, H. (2005). Breaking wave impact force on a vertical and inclined slender pile – theoretical and large-scale model investigations. *Coastal Engineering*, **52**, 435–462.

Wienke, J., Sparboom, U. and Oumeraci, H. (2000). Breaking wave impact on a slender cylinder. In: *Coastal Engineering Conference*, volume 2, 1787–1798.

Wilcox, D.C. (1994). *Turbulence modeling for CFD.* DCW Industries Inc., La Canada, California.

Xie, Z. (2013). Two-phase flow modelling of spilling and plunging breaking waves. *Applied Mathematical Modelling*, **37**, 3698–3713.

Zhao, Q., Armfield, S. and Tanimoto, K. (2004). Numerical simulation of breaking waves by a multi-scale turbulence model. *Coastal Engineering*, **51**(1), 53–80.